Catalysis Science & Technology

Photobiocatalytic H_2 evolution of GaN:ZnO and [FeFe]-hydrogenase recombinant *Escherichia coli*

Journal:	*Catalysis Science & Technology*
Manuscript ID	CY-ART-01-2020-000128.R1
Article Type:	Paper
Date Submitted by the Author:	25-Apr-2020
Complete List of Authors:	KOSEM, NUTTAVUT; Kyushu University International Institute for Carbon-neutral Energy Research; Kyushu University Faculty of Engineering Graduate School of Engineering Department of Applied Chemistry Honda, Yuki; Department of Chemistry, Biology and Environmental Science, Faculty of Science, Nara Women's University Watanabe, Motonori; Kyushu University, International Institute for Carbon-Neutral Energy Research Takagaki, Atsushi; Kyushu University, Applied Chemistry Tehrani, Zahra; Laboratory of Inorganic Chemistry, Department of Chemistry and Applied Biosciences, ETH Zürich Haydous, Fatima; Laboratory of Inorganic Chemistry, Department of Chemistry and Applied Biosciences, ETH Zürich Lippert, Thomas; Paul Scherrer Institut, General Energy Research Department Ishihara, Tatsumi; Kyushu University, Department of Applied chemistry Faculty of Engineering; Kyushu University International Institute for Carbon-neutral Energy Research

PAPER

Photobiocatalytic H_2 evolution of GaN:ZnO and [FeFe]-hydrogenase recombinant *Escherichia coli*

Received 00th January 20xx,
Accepted 00th January 20xx

DOI: 10.1039/x0xx00000x

Nuttavut Kosem,*[a,b] Yuki Honda,[c] Motonori Watanabe,[a] Atsushi Takagaki,[b] Zahra Pourmand Tehrani,[d] Fatima Haydous,[d] Thomas Lippert,[a,d,e] and Tatsumi Ishihara,[a,b]

The need for sustainable, renewable and low-cost approaches is a driving force behind the development of solar-to-H_2 conversion technologies. This study aims to develop new strategy using visible-light photocatalyst coupled to biocatalyst for H_2 production. Photocatalytic methyl viologen (MV^{2+}) reduction activity was investigated to discover active oxynitrides. In comparative studies with $LaTiO_2N$, $BaTaO_2N$ and Ta_3N_5, it was revealed that the suitable surface area, band gap and band edge potentials are some physical factors that responsible for photocatalytic behaviors of GaN:ZnO on MV^{2+} reduction. The activity is enhanced at higher concentrations and alkaline pH of triethanolamine (TEOA). The expression of active [FeFe]-hydrogenase from *Escherichia coli* (Hyd^+ *E. coli*) as a recombinant biocatalyst was confirmed by $MV^{\bullet+}$-dependent H_2 production activity. In the photobiocatalytic system of GaN:ZnO and Hyd^+ *E. coli*, the rate of H_2 production reached the maximum level in the presence of MV^{2+} as an electron mediator at neutral pH as biocompatible condition. The present work reveals a novel hybrid system of H_2 production using visible-light active GaN:ZnO coupled to Hyd^+ *E. coli*, which shows the feasibility to be developed for photobiocatalytic H_2 evolution under solar light.

Introduction

Hydrogen (H_2) acts as a clean energy carrier, with a high-energy capacity of 122 kJ/g, which liberates only water as a by-product of combustion. H_2 is expected to be responsible for 90% of the global fuel in 2080.[1] Currently, 95% of the commercial H_2 is produced from fossil fuel, causing a harmful impact of CO_2 emission.[2] Concerns over fossil fuel decline and the environmental impact of CO_2 emissions are a driving force behind the development of renewable and non-polluting technologies to fulfil the growing energy demand worldwide.

Sunlight, an inexhaustible source, continuously delivers a high amount of energy to the earth. Artificial photosynthetic systems inspired from natural photosynthesis has a great potential for solar energy conversion into chemical fuels.[3] Photobiocatalysis is a novel system, defined as the combination of light-activated photocatalyst coupled to specific enzymes, as biocatalysts for production of chemicals such as H_2.[4]

Over the past few decades, there has been several combinations of inorganic photocatalysts and purified hydrogenase or whole cell bacteria producing hydrogenase, especially [FeFe]-type with high H_2 production activities.[5-8] An example is CdS nanorods capped with 3-mercaptopropionic acid and purified [FeFe]-hydrogenase. This combination showed a photocatalytic reduction of H^+ to H_2, at a turnover frequency of 380-900 s^{-1} with photon conversion efficiency of up to 20%, applying a 405 nm light source.[7] Other photobiocatalytic systems include the use of whole cells, such as wild-type clostridial cells, which produce hydrogenase, that are coupled to TiO_2 under UV illumination.[5] Genetic engineering strategies are used to enhance the efficiencies of the biocatalysts, leading to an increase in intracellular hydrogenase expression.[9] Recently, our group developed a recombinant *E. coli* with the hydA, hydE, hydF, and hydG genes of [FeFe]-hydrogenase from *Clostridium acetobutylicum* NBRG13948, which is known as an efficient biocatalyst for H_2 production.[10] Subsequently, we have reported the first successful combination of P-25 TiO_2 and [FeFe]-hydrogenase-expressing *E. coli* (Hyd^+ *E. coli*), demonstrating an improvement in H_2 production compared to the wild-type strain.[11]

[a] *International Institute for Carbon-Neutral Energy Research (I2CNER), Kyushu University, 744 Motooka, Nishi-ku, Fukuoka 819-0395, Japan. E-mail: kosem_k@i2cner.kyushu-u.ac.jp*
[b] *Department of Applied Chemistry, Faculty of Engineering, Kyushu University, 744 Motooka, Nishi-ku, Fukuoka 819-0395, Japan. E-mail: ishihara@cstf.kyushu-u.ac.jp*
[c] *Department of Chemistry, Biology and Environmental Science, Faculty of Science, Nara Women's University, Kitauoyanishi-machi, Nara 630-8506, Japan. E-mail: honda@cc.nara-wu.ac.jp*
[d] *Laboratory of Inorganic Chemistry, Department of Chemistry and Applied Biosciences, ETH Zürich, CH-8093, Zürich, Switzerland. E-mail: zahra.pourmand-tehrani@psi.ch*
[e] *Laboratory for Multiscale Materials Experiments, Paul Scherrer Institut, Forschungsstrasse 111, CH-5232 Villigen PSI, Switzerland. E-mail: thomas.lippert@psi.ch*

† Electronic Supplementary Information (ESI) available: [Experimental details for construction of recombinant plasmids and [FeFe]-hydrogenase expression in *E. coli*. See DOI: 10.1039/x0xx00000x

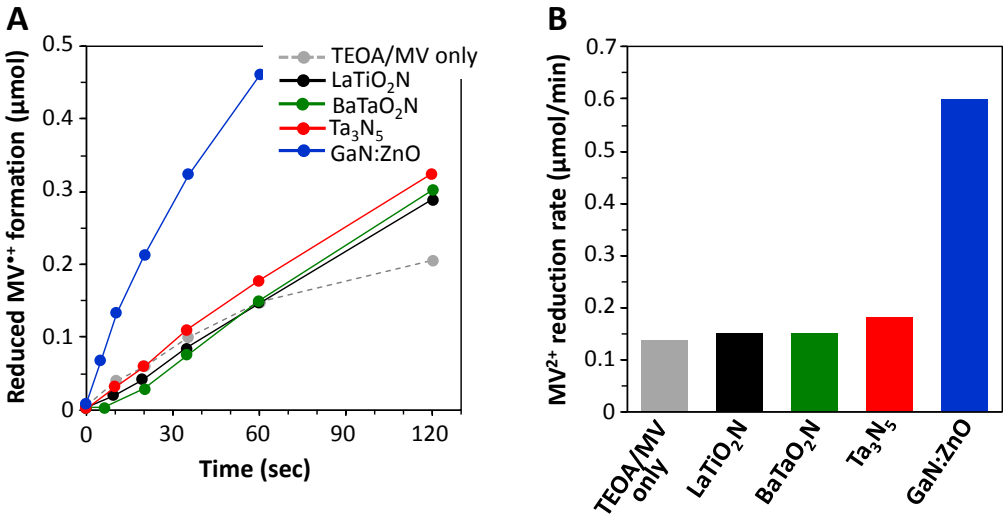

Fig. 1 Photocatalytic MV^{2+} reduction activity of oxynitrides ($LaTiO_2N$, $BaTaO_2N$, Ta_3N_5 and GaN:ZnO) under full arc light source illumination using a 300-W xenon lamp (Fig. S1 in Supplementary Information). Results show the amounts of reduced $MV^{\bullet+}$ in a function of time (A) and MV^{2+} reduction rates of oxynitrides (B).

Most inorganic semiconductors for photocatalytic reactions are metal oxides with wide band gap (>3 eV), requiring UV light for electron excitation.[12,13] However, the solar spectrum at the earth`s surface consists mainly of visible light (44%) and near-infrared light (53%) with a small portion of UV (3%).[14] Metal oxide photocatalysts with band gaps >3 eV do not harvest a large part of the solar spectrum. Thus, there is a significant need to develop visible-light active photocatalysts with high efficiency and strong physico-chemical stability.

One strategy for reducing the band gap of oxide is the partial or full substitution of nitrogen for oxygen. The ionic radius of N^{3-}, which is similar to O^{2-}, facilitates the substitution of nitrogen.[15] Since the report of $La_{1-x}Ca_xTaO_{1+x}N_{2x}$ as a new material[16], various d^0-transition metal (group IIIA-VIA) or d^{10}-typical metal (group IIB-VB) oxynitrides have been discovered. The band gap is reduced (<3 eV) due to the hybridization of O-2p and N-2p orbitals resulting in the upward shift of the valence band maximum, allowing the adsorption of the visible-light energy at 400 nm < λ < 800 nm wavelength in the solar spectrum.[17-20]

To the best of our knowledge, the application of oxynitrides ($LaTiO_2N$, $BaTaO_2N$, Ta_3N_5 and GaN:ZnO) for photobiocatalytic H_2 production has never been studied before. This paper aims to find active oxynitrides with photocatalytic MV^{2+} reduction activity and investigate some physical properties. The optimal conditions for photocatalytic MV^{2+} reduction and photobiocatalytic H_2 production are also studied in an attempt to improve the activities. The expression and activity of [FeFe]-hydrogenase from Hyd^+ *E. coli* are confirmed. Both full arc and visible-light sources are applied to the system for H_2 generation.

Results and discussion

Light reaction: photocatalytic MV reduction

In photochemical reaction, MV^{2+} reduction activity implies the kinetics of electron transfer rate from oxynitrides to MV^{2+} in a function of time determined by monitoring the conversion rate of colorless MV^{2+} (oxidized form) to dark blue $MV^{\bullet+}$ radical (reduced form). The screening was carried out to find active oxynitrides with the potential for MV^{2+} reduction in a reaction mixture consisting of 10% (v/v) TEOA pH 8, 3.33 mg/mL of oxynitride powder, and 5 mM of MV^{2+} solution irradiated by full arc light source (1.7 W/cm^2). A control experiment including only TEOA and MV^{2+} was also carried out to ensure that MV^{2+} reduction is related to the photocatalyst alone. Under the above conditions, GaN:ZnO showed the highest conversion rate of 0.60 µmol/min, which was around 4 times greater

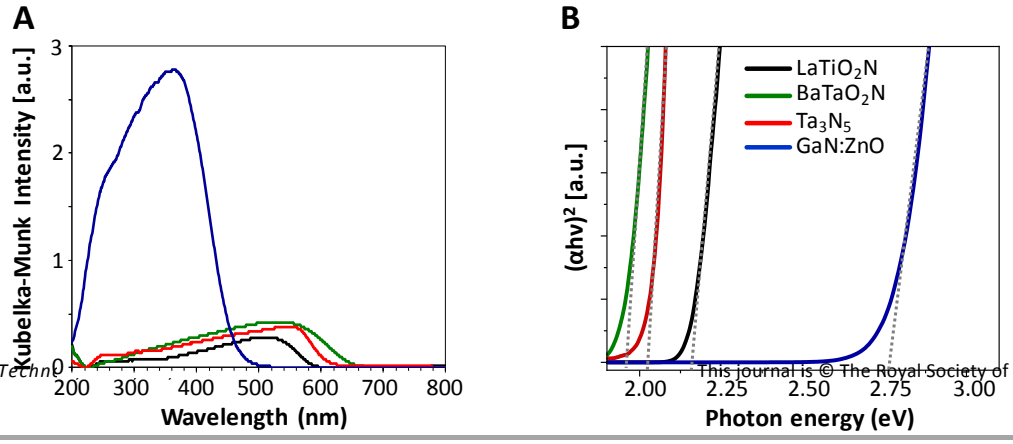

Fig. 2 Kubelka-Munk plots versus wavelength (A) and Tauc plot for band gap energy analysis (B) of oxynitrides, where α is the absorption coefficient of materials, h is the plank`s constant, v is the frequency of light.

PAPER

Table 1 Characterizations of oxynitrides

Oxynitrides	[a] S_{BET} $m^2\ g^{-1}$	[b] Absorption edge nm	[c] E_g eV	[d] E_{CB} (V vs NHE) pH 0 (ph 8)	[e] E_{VB} (V vs NHE) pH 0 (ph 8)	[j] ΔE_e V	[k] ΔE_h V
$LaTiO_2N$	4.2	597	2.14	[f] -0.57 (-1.042)	[f] 1.54 (1.068)	0.602	0.057
$BaTaO_2N$	2.1	670	1.95	[g] -0.38 (-0.852)	[g] 1.59 (1.118)	0.412	0.107
Ta_3N_5	5.6	628	2.03	[h] -0.52 (-0.992)	[h] 1.58 (1.108)	0.552	0.097
GaN:ZnO	7.3	486	2.77	[i] -0.60 (-1.072)	[i] 2.17 (1.698)	0.632	0.687

[a] S_{BET} is the surface area by the BET method. [b] Absorption edge obtained from the UV-visible diffuse reflectance spectra. [c] E_g is the band gap energy estimated from the extrapolation of Tauc plot versus photon energy. [d] E_{CB} is the conduction band edge potential and [e] E_{VB} is the valence band edge potential. E_{CB} and E_{VB} values at pH 0 were obtained from the literature; [f] Ref (22), [g] Ref (23), [h] Ref (24), [i] Ref (25), while the values at pH 8 in parentheses were estimated from the Nernst Equation ($E = E^0 - 0.059$pH). [j] $\Delta E_e = E(MV^{2+}/MV^{\bullet+}) - E_{CB}$ and [k] $\Delta E_h = E_{VB} - E(TEOA/TEOA^+)$ are the calculation of respective overpotentials. $E(MV^{2+}/MV^{\bullet+}) = -0.44$ is the redox potential of methyl viologen and $E(TEOA/TEOA^+) = 1.011$ is the redox potential of triethanolamine estimated at pH 8.

than Ta_3N_5 (0.18μmol/min), $BaTaO_2N$ (0.15 μmol/min) and $LaTiO_2N$ (0.15 μmol/min) (Fig. 1). Compared to the activity of TEOA solution alone as a negative control (0.14 μmol/min), the electron transfer from $LaTiO_2N$, $BaTaO_2N$ and Ta_3N_5 to MV^{2+} are negligible.

It is generally known that functionality of material is strongly dependent on its physicochemical characteristics.[13] Therefore, investigating the relationship between photocatalytic activity and basic characterizations of material is an essential issue in the development of highly active oxynitrides.

X-ray diffractograms characterized at 2θ degree confirm the crystalline structure of individual oxynitrides determined in this study as shown in Fig. S3 of the Supplementary Information. Among oxynitrides, GaN:ZnO with MV^{2+} reduction activity exhibits the largest surface area per mass (7.3 $m^2\ g^{-1}$), while $LaTiO_2N$, $BaTaO_2N$ and Ta_3N_5 with smaller surface area have no activity. The correlation of surface area and photocatalytic activity has been also found in many metal-oxide materials. It was found that lower activity with decreasing surface area was attributed to a decrease in the number of reaction sites on the catalyst surface.[21] Therefore, GaN:ZnO with higher surface area may facilitate photocatalytic efficiency on MV^{2+} reduction activity.

Investigations on UV-vis diffuse reflectance spectrophotometry have provided the absorption edge and band gap energy. In Table 1, the absorption edges of all oxynitrides were observed in the visible region (> 400 nm), indicating their visible-light absorption properties. The band gap energy (E_g) was evaluated from Tauc plot extrapolation as shown in Fig. 2B and Table 1. $LaTiO_2N$, $BaTaO_2N$ and Ta_3N_5 show the similar E_g values at around 2 eV, while the E_g value of GaN:ZnO was estimated to be 2.77 eV. The experimental results confirm that all oxynitrides have the band gap narrower than 3 eV that sufficiently small to allow the visible-light absorption.[13-17]

In addition, it was found that the evaluated band gap values are consistent with their band edge potentials in the published literatures[22-25] as shown in Table 1. It is well known that the band edge must be located in a position that allows for the reduction and oxidation of water by photoexcited electrons and holes.[26] In case of photocatalytic MV^{2+} reduction, it can be achieved when the conduction band edge potential (E_{CB}) of material is more negative than the redox potential of MV^{2+} as an electron acceptor, $E_{CB} < E(MV^{2+}/MV^{\bullet+})$. While the valence band edge potential (E_{VB}) must be more positive than the redox potential of an electron donor (D), $E_{VB} > E(D/D^{\bullet+})$.[26,27]

The rate of interfacial electron transfer was presented in terms of the respective overpotential as follows:

$$\Delta E_e = E(MV^{2+}/MV^{\bullet+}) - E_{CB}$$

$$\Delta E_h = E_{VB} - E(TEOA/TEOA^{\bullet+})$$

where ΔE_e indicates the electron transfer rate of the conduction band electrons (e^-_{CB}) to the acceptor MV^{2+}, while ΔE_h indicates the electron transfer rate of the valence band holes (h^+_{VB}) to the electron donor TEOA.[27]

As MV^{2+} reduction activity was determined at pH 8, the estimated E_{CB} and E_{VB} values were shown in Table 1. The results show that all oxynitrides have E_{CB} more negative than the redox potential of methyl viologen (< -0.44 V vs NHE)[27,28] and E_{VB} more positive than that of TEOA (> ca. 1.011 V vs NHE)[29] at pH 8. Compared with other materials, GaN:ZnO shows the highest rates of interfacial electron transfer with the respective overpotentials ΔE_e and ΔE_h of 0.632 V and 0.687 V, respectively. Therefore, the increase in MV^{2+} reduction activity is considered to be associated with the optimum E_{CB} and E_{VB} values of materials.

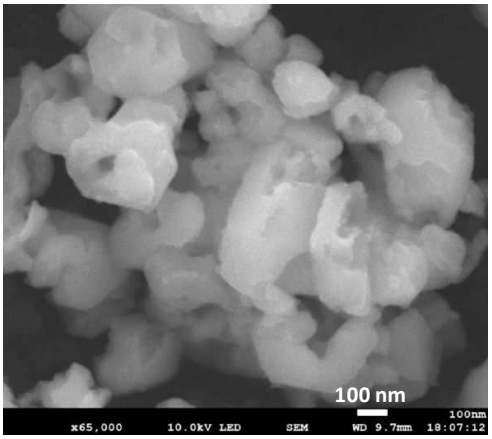

Fig. 3 SEM image of GaN:ZnO.

The results presented here reveal that differences in surface area, band gap energy and band edge potentials (E_{CB} and E_{VB}) are responsible for photocatalytic behaviors of oxynitrides. GaN:ZnO with the strongest MV^{2+} reduction activity was selected for next experiments in this study. X-ray diffraction analysis clearly confirms the crystalline formation of GaN:ZnO solid solution (Fig. S3 D in the Supplementary Information) with XRD pattern similar to those of GaN and ZnO.[30-32] In Fig. 3, SEM image displays the well-crystallized particles of GaN:ZnO with average particle size of 320 nm, which prepared from the mixture of β-Ga_2O_3 and ZnO under NH_3 flow at 1123 K for 15 h. It was reported that more regular and larger shaped crystallization gradually proceeded during nitridation period resulted from the formation of wurtzite crystal structure.[32]

According to the results, the reaction mechanism of MV^{2+} reduction by GaN:ZnO can be proposed as follows:

$$\text{TEOA} + \text{GaN:ZnO} \xrightarrow{h\nu} \text{GaN:ZnO*}(h^+_{VB} + e^-_{CB}) + \text{TEOA}^+ \quad (1)$$

$$e^-_{CB} + MV^{2+}\,(\text{colorless}) \rightarrow MV^{\bullet+}\,(\text{blue}) \quad (2)$$

The excitation of GaN:ZnO* by light source (*hv*) generates the valence band hole (h^+_{VB}) and conduction band electron (e^-_{CB}) species (1). The photoinduced e^-_{CB} on the surface of GaN:ZnO* are transformed to MV^{2+} and then turned to the reduced $MV^{\bullet+}$ (2).

To understand the role of each component, MV^{2+} reduction was carried out in various conditions. The effect of GaN:ZnO concentration was determined as shown in Fig. 4A. An increase in MV^{2+} reduction rate was observed from 0.35 – 0.55 μmol/min by GaN:ZnO concentrations at 0.33 and 1.67 mg/mL, while no significant enhancement was found using GaN:ZnO at higher concentrations. The similar phenomenon has been reported in the reaction of Au/TiO_2 photocatalyst and methanol for H_2 production. A decrease of H_2 production is associated to the excess of photocatalyst particles in the reaction. It tends to agglomerate and form larger particles, obstructing light scattering and the proper activation of photocatalysts.[33]

MV^{2+} is water soluble and widely utilized to accept photoinduced e^-_{CB} from the conduction band of photocatalysts.[34] By accepting e^-_{CB}, charge separation is promoted and the simultaneous e^-_{CB}/h^+_{VB} recombination is prevented. To investigate this phenomena, the effect of the MV^{2+} concentration on its own reduction rate has been studied. In Fig. 4B, the reduction rate was enhanced around 40% from 1 mM (0.41 μmol/min) to 5 mM (0.58 μmol/min), which is followed by a small increase of a 10 mM MV^{2+} (0.63 μmol/min).

Previous reports on measuring the electron-transfer quantum yield induced by laser-pulse-irradiated colloidal semiconductors also revealed a similar relationship between the formation of $MV^{\bullet+}$ radicals and the concentration of MV^{2+}. By changing the concentration, the quantum yield of MV^{2+} reached the maximum at small initial concentrations and gradually decayed at higher concentrations.[35] Rapid electron-transf.er at small initial concentrations could be due to the adsorption of MV^{2+} molecules on the surface of the semiconductor particles. However, it can be saturated at higher concentrations, resulting in delayed the reaction.[36] Moreover, the decay of surface-adsorbed MV^{2+} molecules at higher concentration can be attributed to the formation of MV^{2+} dimers.[37] As MV^{2+} dimerization highly depends on viologen contents in the reaction, a suitable concentration of 5 mM MV^{2+} was selected for experiments.

Due to the rapid recombination of photoexcited e^-_{CB} and h^+_{VB}, it is difficult to achieve water-splitting directly for H_2 generation using photocatalysts in water.[26] Thus adding sacrificial reagents as electron donors or h^+_{VB} scavengers is critical for promoting the photocatalytic e^-_{CB}/h^+_{VB} separation, which results in higher quantum efficiencies.[38-40] In this study, TEOA is utilized as an electron donor with a redox potential of ca. 1.011 V vs NHE at pH 8 that can be oxidized by h^+_{VB}.[29] Under identical conditions, the effect of TEOA concentrations in the suspension including GaN:ZnO (3.33 mg/mL) and MV^{2+} (5 mM) has been investigated. Fig. 4C displays that the rate of MV^{2+} reduction significantly relies on the TEOA concentrations. The rate increases

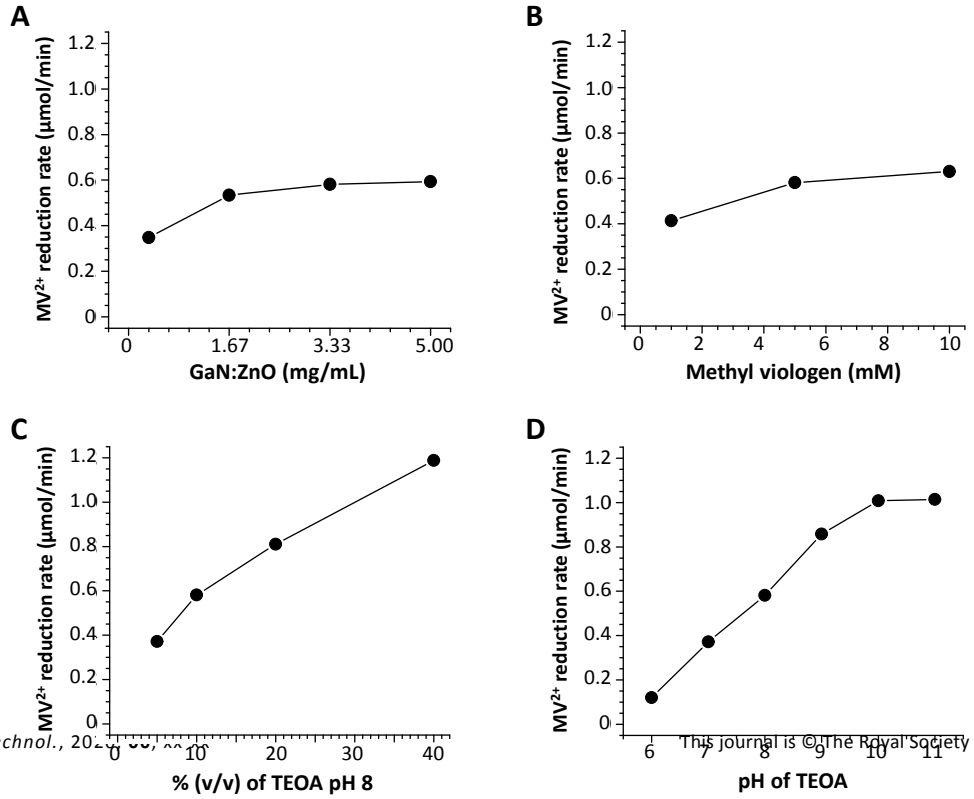

Fig. 4 Photocatalytic MV^{2+} reduction of GaN:ZnO in various conditions: different concentrations of GaN:ZnO (A), MV^{2+} (B), TEOA (C) and different pH of TEOA (D). The reactions were initiated with full arc using a 300-W xenon lamp as a light source (Fig. S1 in Supplementary Information).

sharply from 0.4 to 1.2 μmol/min in the presence of 5% to 40% TEOA at pH 8, respectively. It indicates that the h^+_{VB} scavenging could be the efficiency-limiting step of the process.

It was reported that MV^{2+} reduction activity depends on the adsorption of the three polar-OH groups of TEOA on the surface of TiO_2, which facilitates the direct electron transfer from the sacrificial reagent to the photocatalyst particles.[41] Upon the photocatalytic reaction, TEOA will be oxidized by the holes at the valence band and all three N-C bonds will be decomposed to yield ammonia, formaldehyde, H_2 and other products.[40,42] This can be described by a Langmuir-Hinshelwood-type law, in which the reduction rate depends on the adsorption coefficient of the sacrificial reagent on the surface of the photocatalyst, the surface pseudo-first order rate constant, and the concentration of sacrificial reagent.[42] According to this rational, the surface of GaN:ZnO are fully covered with TEOA at higher concentrations, thus obstructing the recombination of photogenerated e^-_{CB}/h^+_{VB}.

The influence of different pH values on the MV^{2+} reduction rate was also determined. As shown in Fig. 4D, under identical condition of the reaction suspension including 10% (v/v) TEOA, 3.33 mg/mL GaN:ZnO, and 5 mM MV^{2+}, the rates of $MV^{\bullet+}$ formation strongly depend on the pH. The rate increases from pH 6 (0.12 μmol/min) to pH 10 (1.01 μmol/min), and reaches a constant value at pH >10. The results show higher MV^{2+} reduction rates in alkaline pH, while lower activities in acidic condition are observed.

This phenomenon is attributed to the acid-base equilibrium of TEOA. The protonation of $TEOA^+$ in acidic conditions can take an electron from the reduced $MV^{\bullet+}$, provoking the back reaction and consequently lead to the decay of $MV^{\bullet+}$. In alkaline suspensions, the deprotonation of $TEOA^+$ predominantly yields a neutral TEOA radical with an unpaired electron in α-position to either an amino or alcohol group. Such species with strong reducing properties mainly provide electrons and refrain from the competing $MV^{\bullet+}$ reoxidation. Therefore, there is a high increase in $MV^{\bullet+}$ formation in alkaline condition.[43]

AQY is represented to investigate the quantitative relationship between the photoinduction of GaN:ZnO at specific wavelength irradiation for MV^{2+} reduction. AQY% is defined as the ratio of reduced $MV^{\bullet+}$ formed per photon of light absorbed by the photocatalyst at a given wavelength.[13]

In Fig. 5A, MV^{2+} reduction rates of GaN:ZnO are lower than that of P-25 in the UV region. AQYs of GaN:ZnO are 1.88% at 350 nm and 1.15% at 390 nm. On the other hand, photoexcited GaN:ZnO promotes higher MV^{2+} reduction rates than P-25 in the visible-light region with AQYs of 0.93%, 0.37% and 0.18% using 420-nm, 470-nm and 500-nm bandpass filters, respectively (Table S1 and S2 in the Supplementary Information).

Fig. 5B depicts AQYs as a function of wavelength from 350–500 nm. GaN:ZnO responds to visible-light wavelength up to 520 nm, corresponding well to its UV-Vis spectrum with longer absorption edge as compared to the metal oxide P-25 TiO_2 which has an absorption edge around 400 nm.[44,45] Therefore, it is evident that GaN:ZnO is more suitable for visible-light absorption.

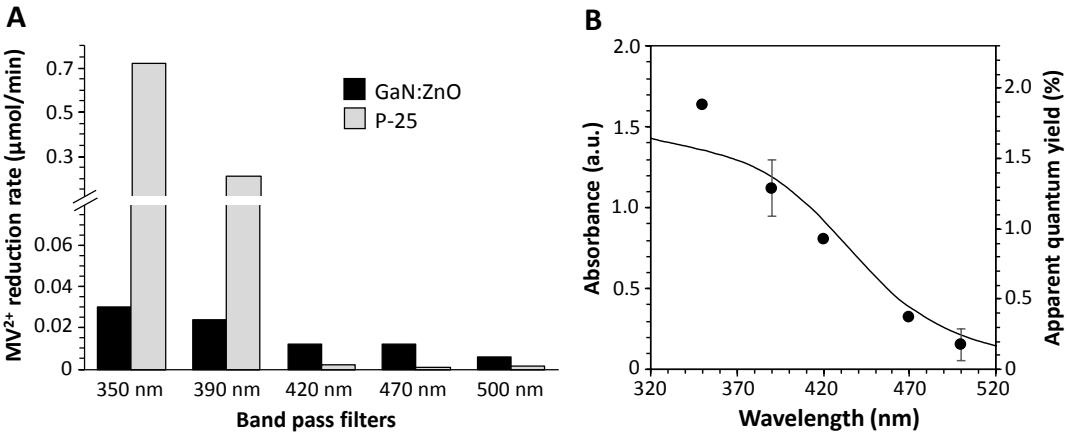

Fig. 5 Apparent quantum yield (AQY) analysis based on photocatalytic MV^{2+} reduction under individual wavelength irradiation. MV^{2+} reduction rate of GaN:ZnO compared with P-25 at given wavelengths (A). AQY% was overlaid with the UV-Vis absorption spectrum of GaN:ZnO in a function of wavelengths (B) based on the calculation in Table S1 and S2 in the Supplementary Information.

PAPER

Dark reaction: biocatalytic H_2 production

After transformation process, it was found that only the colonies of cells carrying pEHydEA with ampicillin resistant gene and pCHydFG with streptomycin resistant gene could grow on the medium containing the antibiotics after 20 h incubation (Fig. S4 in the Supplementary Information). To confirm the successful transformation, both plasmids were extracted from Hyd$^+$ cells and observed by agarose gel electrophoresis. In Fig. 6A, pEHydEA and pCHydFG recombinant plasmids were observed on Lane 4 compared to standard pEHydEA (8.2 kbp) on Land 2 and pCHydFG (6.4 kbp) on Land 3.

the reaction was performed under anaerobic condition. It was shown in Fig. 6B that the reaction of Hyd$^+$ cells and reduced MV$^{\bullet+}$ shows H_2 production rate at 1.72 μmol H_2 h^{-1} from 10 mg-cell, whereas no H_2 was detected from Hyd$^-$ cells. The results confirm that Hyd$^+$ *E. coli* expressing [FeFe]-hydrogenase can be served as an active biocatalyst for H_2 production. The following reaction mechanism is proposed in accordance with the results:

$$\text{Hyd}^+ \textit{ E. coli} + \text{MV}^{\bullet+} + \text{H}^+ \xrightarrow{\text{[FeFe] - Hydrogenase}} \text{Hyd}^+ \textit{ E. coli} + \text{MV}^{2+} + \frac{1}{2}\text{H}_2 \quad (3)$$

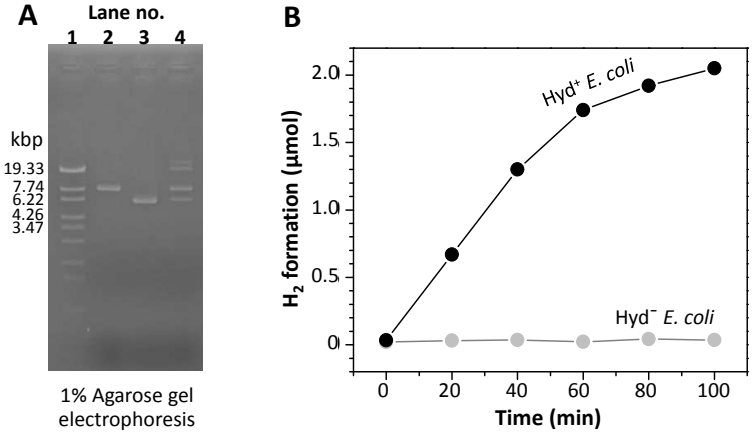

Fig. 6 The presence of co-transformed plasmids and [FeFe]-hydrogenase activity in Hyd$^+$ *E. coli*. Agarose gel electrophoresis (A) shows the λ/Sty I digest Marker in Lane 1, pEHydEA standard in Lane 2, pCHydFG standard in Lane 3 and the extracted plasmids from Hyd$^+$ *E. coli* in Lane 4. Hydrogenase activities of Hyd$^+$ (●) and Hyd$^-$ (●) *E. coli* were determined by MV$^{\bullet+}$-dependent H_2 production activity (B).

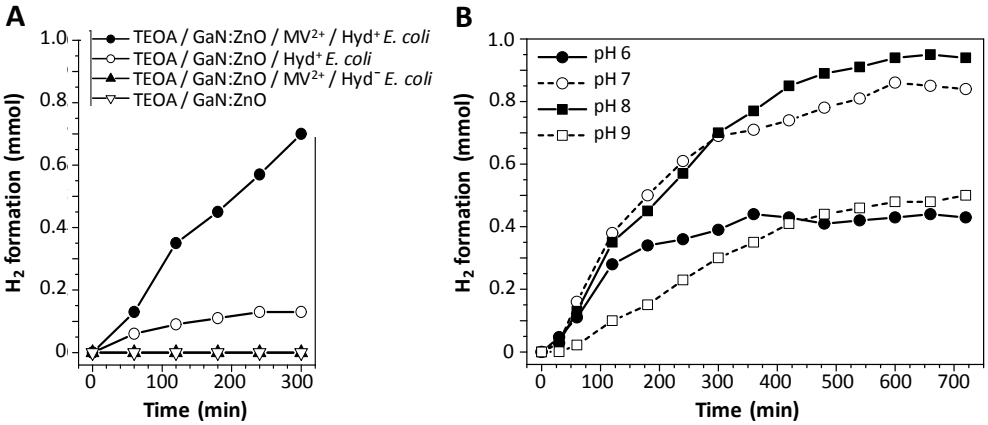

Fig. 7 Photobiocatalytic H_2 formation of GaN:ZnO coupled to Hyd$^+$ *E. coli* irradiated by full arc light source using a 300-W xenon lamp. Data show the amounts of H_2 formed in different conditions (A). The effect of pH on H_2 production was investigated in the reaction system including 50 mg of GaN:ZnO, 5 mM of MV^{2+}, 0.1 g of Hyd$^+$ *E. coli* and 10% (v/v) of TEOA in different pH (B).

However, to make sure that Hyd$^+$ cells express an active [FeFe]-hydrogenase, its activity was determined based on MV$^{\bullet+}$-dependent H_2 production. To avoid O_2 in air that inactivate hydrogenase activity,

Hybrid system of photobiocatalytic H_2 production

Photobiocatalytic H_2 production from the coupling of GaN:ZnO and Hyd$^+$ *E. coli* was determined. As O_2 inactivates [FeFe]-hydrogenase

and MV^{2+} reduction activities, all experiments were performed in anaerobic environment. H_2 generation was monitored in aqueous suspension of the complete system including 10% (v/v) TEOA pH 8, 2.5 mg/mL of GaN:ZnO, 5 mM MV^{2+}, and 0.1 g wet weight of Hyd^+ *E. coli* under full arc illumination (0.9 W/cm^2). As shown in Fig. 7A, the maximum amount of H_2 was generated in the presence of all four components with a rate of 162.9 µmol/h. While the reaction consisting of only TEOA and GaN:ZnO produced almost no H_2. An irradiated solution of the complete system maintains the dark blue color indicating the presence of reduced $MV^{\bullet+}$ after prolonged, i.e. 12-hour, experiments. The exclusion of MV^{2+} in the system led to a 2-fold decrease in the production rate, which did not exceed 48 µmol/h after 5 h illumination. The result confirmed the role of MV^{2+} as an effective electron mediator. The enhancement is due to cell membrane permeability of $MV^{\bullet+}$ and subsequently e^- transfer to protons (H^+) at the active site of [FeFe]-hydrogenase for H_2 generation.[46] In the reaction using Hyd^- *E. coli* without [FeFe]-hydrogenase expression, H_2 production is negligible.

The effect of the pH on the biocatalytic function of [FeFe]-hydrogenase was studied by experiments at various pHs of TEOA. Fig. 7B shows that the most suitable pH was observed in the system of 10% (v/v) TEOA pH 7 and 8 with H_2 formation rates of 179.5 and 162.9 µmol/h, respectively. The system is less efficient at acidic and alkaline environments with the rates of 131.3 and 42.7 µmol/h for pH 6 and 9, respectively. Although the strong intensity of reduced $MV^{\bullet+}$ obtained from photocatalytic reaction was promoted in alkaline condition, higher H_2 formation rates are obtained at pH 7 and 8 as biocompatible condition, which preserves the function and structural integrity of bacterial cells and enzymes. Strong acidic and alkaline environments are toxic to the bacteria and can denature the structure, resulting in enzyme dysfunction. Thus, neutral pH must be employed in photobiocatalytic systems, as a more stable condition for conserving the [FeFe]-hydrogenase activity and *E. coli* cell integrity.

In addition, experiments were also carried out under visible light using a 300-W xenon lamp equipped with a 422-nm longpass filter

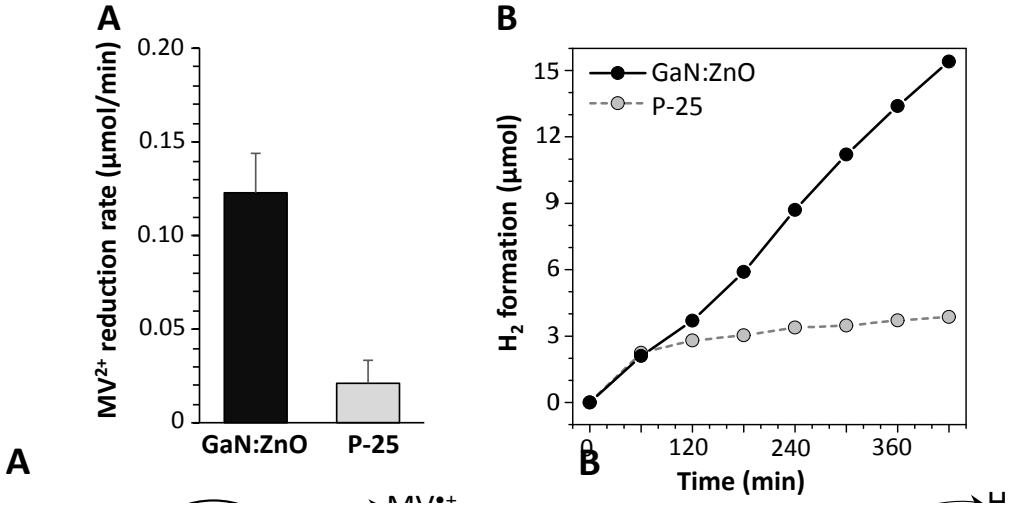

Fig. 8 The activities of GaN:ZnO under visible-light irradiation. MV^{2+} reduction (A) and photobiocatalytic H_2 production of GaN:ZnO coupled with Hyd^+ *E. coli* (B) compared to P-25 using a 300 W xenon lamp equipped with UV cutoff filter (λ ≥ 422 nm) as a light source.

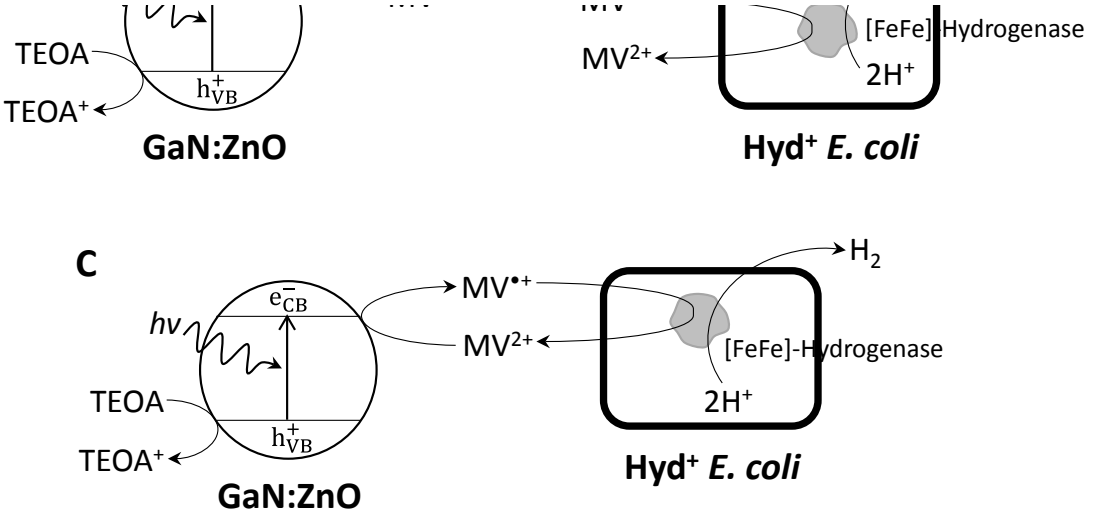

Scheme 1 The reaction mechanisms of photocatalytic MV^{2+} reduction of GaN:ZnO (A), biocatalytic H_2 production of Hyd^+ *E. coli* (B), Hybrid photobiocatalytic H_2 evolution of GaN:ZnO coupled to Hyd^+ *E. coli* (C). Hyd^+ *E. coli* indicates [FeFe]-hydrogenase expressing *E. coli*.

(0.25 W/cm^2). Photocatalytic MV^{2+} reduction was observed with the rates of 0.12 and 0.02 µmol/min for GaN:ZnO and P-25, respectively (Fig. 8A). For photobiocatalytic H_2 production of the complete reaction system (20 mL) including: 10% (v/v) TEOA pH 8, 2.5 mg/mL GaN:ZnO, 5 mM MV^{2+}, and 0.1 g of Hyd^+ *E. coli*, H_2 was evolved with the rates of 2.26 and 0.44 µmol/h for GaN:ZnO and P-25, respectively (Fig. 8B). The visible light energy is sufficient to excite electron from the valence band to the conduction band of GaN:ZnO for promoting both MV^{2+} reduction and photobiocatalytic H_2 production.

Conclusions

The coupling of GaN:ZnO to Hyd^+ cells is a novel artificial photobiocatalytic system for H_2 production. In the light reaction (Scheme 1A), photocatalytic MV^{2+} reduction rate mainly depends on both the concentration and pH of TEOA as a sacrificial electron donor. In addition, studies on oxynitrides with different physical properties reveal that the suitable surface area, band gap and band edge potentials (E_{CB} and E_{VB}) of GaN:ZnO are responsible for photocatalytic MV^{2+} reduction. Understanding on the role of these features may guide to improve more efficient oxynitrides in the future. In Scheme 1B, the dark reaction confirms that recombinant Hyd^+ *E. coli* expresses an active [FeFe]-hydrogenase for H_2 generation. The proposed mechanism of hybrid photobiocatalytic system is illustrated as shown in Scheme 1C including TEOA, GaN:ZnO, MV^{2+} and Hyd^+ *E. coli*. The reduced $MV^{\bullet+}$ penetrates through the cell membrane, transferring e^- to H^+ and producing H_2 via the activity of intracellular [FeFe]-hydrogenase. Although photocatalytic MV^{2+} reduction was found to be increased at alkaline pH, the highest efficiency of photobiocatalytic H_2 production was observed at neutral pH as biocompatible condition, which is suitable to preserve cell integrity and the function of [FeFe]-hydrogenase. This investigation is a novel approach in constructing artificial photobiocatalytic system for H_2 production under visible light irradiation using visible-light absorbed GaN:ZnO coupled to Hyd^+ *E. coli*. However, the system should be improved to enhance the stability and efficiency, especially for a large-scale production under solar light in the future.

Experimental

General

Triethanolamine (TEOA; >98.0%, Wako) and 1,1'-dimethyl-4,4'-bipyridium dichloride (methyl viologen; >98.0%,) were purchased from Tokyo Chemical Industry Co., Ltd. Ga2O3 (99.99%) and ZnO (99.99%) powders were purchased from Koujundo Chemical Lab. Co., Ltd. High-purity water (<0.055 µS/cm) was supplied by an ultrapure water system (RFU424TA, Advantec) for all chemical preparations.

Oxynitride preparation

$LaTiO_2N$ powders were prepared using the solid-state method by heating a stoichiometric mixture of La_2O_3 and TiO_2 at 1150°C in the presence of NaCl flux for 5 h. Thermal ammonolysis of the obtained oxide at 950°C for 16 h under ammonia flow (250 mL/min) resulted in $LaTiO_2N$ oxynitride powder.[19]

$BaTaO_2N$ preparation was carried out by the thermal ammonolysis of $Ba_5Ta_4O_{15}$ at 950°C for 16 h. $Ba_5Ta_4O_{15}$ was prepared by the solid-state route from $BaCO_3$ and Ta_2O_5 without flux followed by annealing at 1000°C for 10 h.[20]

Ta_3N_5 powders were prepared by subjecting the Ta_2O_5 precursor to nitridation under a flow of NH_3 gas. The nitridation was conducted at 900°C for 24 hour under an NH_3 flow of 250 mL/min.[24]

GaN:ZnO powder was prepared according to previous reports. Nitridation of a mixture of Ga_2O_3 (1.35 g) and ZnO (1.173 g) was performed by heating the oxides under an NH_3 gas flow (99.8%, 200 mL/min flow rate) at 1123 K for 15 h on an alumina boat, resulting in a yellow powder.[47,48]

Specific surface area was analysed by the Brunauer–Emmett–Teller (BET) method via N_2 physical adsorption at -196°C in liquid N_2 on a BELsorp(II)-mini (BEL Japan, INC.). The samples were pretreated to remove moisture at 150°C for 2 h in high vacuum (BELprep(II)-vac, BEL Japan, INC.). The optical properties of photocatalysts were characterised with a Shimadzu UV-3600 Spectrophotometer in the wavelength range of 200–800 nm using barium sulphate as reference. The collected reflectance spectra were converted to absorbance using the Kubelka-Munk transformation and used for band-gab energy evaluation. The morphologies of photocatalysts were observed by scanning electron microscopy (SEM, JSM-7900F, JEOL). X-ray diffraction was performed using the powder diffraction method (RINT2500HLR+, Rigaku Corporation).

Photocatalytic methyl viologen (MV^{2+}) reduction

The reaction mixture consisted of 10% (v/v) TEOA pH 8, 3.33 mg/ml of the inorganic semiconductor and 5 mM MV^{2+} aqueous solution. A total volume of 3 mL reaction solution was used for an experiment. Blank experiments including 10% (v/v) TEOA and 5 mM MV^{2+} without the semiconductors are also done under similar conditions. The reaction is conducted in a 10 mm × 10 mm quartz cuvette with a screw cap with a polytetrafluoro-ethylene/silicone septum. O_2 was displaced by bubbling N_2 gas through the solution for 20 min. The reaction was initiated by light irradiation using a 300-W xenon illuminator (Fig. S1 in the Supplementary Information), and the absorption spectra were monitored using a spectrophotometer (SH-1000Lab, Corona Electric Co., Ltd., Japan). The cuvette was then centrifuged (1,000 ×g for 1 min) to avoid the diffusion of inorganic semiconductor powder. The amount of reduced $MV^{\bullet+}$ formed was calculated from the absorbance at 605 nm using a molar conversion coefficient, ε, of 1.3×10^4 $M^{-1}cm^{-1}$.[11,49]

Apparent quantum yields (AQYs) for photocatalytic MV reduction

AQYs experiments were conducted in the same reaction condition including: 10% (v/v) TEOA pH 8, 3.33 mg/mL of the inorganic semiconductor (GaN:ZnO or P-25), and 5 mM MV^{2+}. To measure AQYs[11], the reaction was initiated by heatless monochromatic illumination using MAX-303, 300-W xenon light source (Asahi Spectra) with optical filters for selected wavelengths (300 ± 5, 350 ± 5, 390 ± 5, 420 ± 5, 470 ± 5 and 500 ± 5 nm). The spectra of the reduced $MV^{\bullet+}$ was obtained using a spectrophotometer. The light intensity of each wavelength was measured to calculate the number of incident photons by an intensity detector. The AQYs for photocatalytic MV^{2+} reduction are defined as shown below:

$$\text{AQY\%} = 100 \times \frac{\text{Rate of reduced } MV^{\bullet+} \ (\text{mol s}^{-1})}{\text{Rate of incident photons } (\text{mol s} - 1)}$$

Recombinant Hyd^+ *E. coli* construction and cultivation

Co-transformation of two recombinant plasmids (pEHydEA and pCHydFG) encoding [FeFe]-hydrogenase (HydA) and maturase (HydE, HydF and HydG) genes from *Clostridium acetobutylicum* NBRC 139482 were used to constructed recombinant *E. coli* according to a previous method.[9,10,50] The recombinant *E. coli* BL21(DE3)/pEHydEA + pCHydFG was applied as a living biocatalyst. It was aerobically pre-cultured in 200 mL of LB Miller broth supplemented with 100 μg/mL of ampicillin, 40 μg/mL of streptomycin, 0.5% (w/v) of glucose, 250 μg/mL of ferric ammonium citrate and 100 mM MOPS/NaOH (pH 7.4) at 37°C, 120 rpm until the cell density reached an optical density of 0.4 at 600 nm (OD600). The cultures were then transferred into an anaerobic glove box (MIWA MFG Co., Ltd., Osaka, Japan) supplemented with 2 mM L-cysteine, 25 mM sodium fumarate and 0.1 mM isopropyl-β-D-thiogalactopyranoside (IPTG). The cell pellet was harvested and resuspended in sterile water. The cell wet weights were estimated before the experiments.

Determination of hydrogenase activity

After cultivation, freshly harvested cells were washed and resuspended in 10 mM phosphate buffer pH 7. [FeFe]-hydrogenase activity was determined by MV-dependent H_2 evolution assay. In a 10-mL sealed glass vial, the reaction was initiated by adding 5 mM reduced $MV^{\bullet+}$ (MV^{2+} dissolved in sodium dithionite) into the vial containing 10 mg of wet cells suspended in the phosphate buffer under N_2 atmosphere. After incubating at 37°C for 1 h, the reaction was terminated by adding 10% trichloroacetic acid solution. The amount of H_2 was monitored by a gas chromatograph (GC; GC-8A, Shimadzu Corp., Japan) equipped with a thermal conductivity detector and an integrator C-R6A (Shimadzu Corp.) The reaction gas went through a molecular sieve 5A column (GL Sciences Inc., Japan) with argon as a carrier gas.

Photobiocatalytic H_2 production

A 20-mL reaction mixture, consisting of 10% (v/v) of TEOA, 5 mM of MV^{2+}, 50 mg of oxynitride powder and 0.1 g-wet weight of Hyd^+ *E. coli*, was mixed in a quartz reactor under anaerobic conditions (97% N_2 and 3% H_2 atmosphere, O_2 <1 ppm). After the reactor was connected to a closed gas circulation system, the atmosphere of the reaction system was evacuated and replaced with argon to remove N_2 and H_2. A dark reaction was first performed to confirm that there was no gas leakage. After light irradiation, the yield of H_2 was monitored by a gas chromatograph (GC; GC-8A, Shimadzu Corp., Japan) with argon as carrier gas, equipped with a thermal conductivity detector and an integrator C-R6A (Shimadzu Corp.) The reaction gas went through a molecular sieve 5A column (GL Sciences Inc., Japan) and a gas sampler that was directly connected to the reactor.[11]

Conflicts of interest

There are no conflicts to declare.

Acknowledgements

This work was supported by the International Institute for Carbon-Neutral Energy Research (WPI-I2CNER), which was established by the World Premier International Research Center Initiative (WPI), MEXT and the Strategic International Collaborative Research Program (SICORP) in "Research on hydrogen as a renewable energy carrier'' from Japan Science and Technology Agency (JST), Japan. The acknowledgements come at the end of an article after the conclusions and before the notes and references.

Notes and references

1 T. da S. Veras, T. S. Mozer, D. da C. R. M. dos Santos and A. da S. César, *Int. J. Hydrogen Energy*, 2017, **42**, 2018–2033.
2 P. Nikolaidis and A. Poullikkas, *Renew. Sustain. Energy Rev.*, 2017, **67**, 597–611.
3 G. W. Crabtree and N. S. Lewis, *Phys. Today*, 2007, **60**, 37–42.
4 J. A. Maciá-Agulló, A. Corma and H. Garcia, *Chem. Eur. J.*, 2015, **21**, 10940–10959.
5 A. A. Krasnovsky and V. V. Nikandrov, *FEBS Lett.*, 1987, **219**, 93–96.
6 V. V. Nikandrov, M. A. Shlyk, N. A. Zorin, I. N. Gogotov and A. A. Krasnovsky, *FEBS Lett.*, 1988, **234**, 111–114.
7 K. A. Brown, M. B. Wilker, M. Boehm, G. Dukovic and P. W. King, *J. Am. Chem. Soc.*, 2012, **134**, 5627–5636.
8 P. W. King, *Biochim. Biophys. Acta*, 2013, **1827**, 949–957.
9 S. Kim, D. Lu, S. Park and G. Wang, *Int. J. Hydrog. Energy*, 2012, **37**, 15833–15840.
10 Y. Honda, H. Hagiwara, S. Ida and T. Ishihara, *Angew. Chem. Int. Ed.*, 2016, **55**, 8045–8048.
11 Y. Honda, M. Watanabe, H. Hagiwara, S. Ida and T. Ishihara, *Appl. Catal. B: Environ.*, 2017, **210**, 400–406.
12 X. Chen, S. Shen, L. Guo and S.S. Mao, *Chem. Rev.*, 2010, **110**, 6503–6570.
13 A. A. Ismail and D. W. Bahnemann, *Sol. Energy Mater. Sol. Cells*, 2014, **128**, 85–101.
14 D. M. Schultz and T. P. Yoon, *Science*, 2014, **343**, 958–993.
15 T. Takata, C. Pan and K. Domen, *Sci. Technol. Adv. Mater.*, 2015, **16**, 1–18.
16 M. Jansen and H. P. Letschert, *Nature*, 2000, **404**, 980–982.

17 J. Kubota and K. Domen, *Electrochem. Soc. Interface*, 2013, **22**, 57–62.
18 S. Banerjee, S. C. Pillai, P. Falaras, K. E. O'Shea, J. A. Byrne and D. D. Dionysiou, *J. Phys. Chem. Lett.*, 2014, **5**, 2543–2554.
19 M. Pichler, W. Si, F. Haydous, H. Téllez, J. Druce, E. Fabbri, M. E. Kazzi, M. Döbeli, S. Ninova, U. Aschauer, A. Wokaun, D. Pergolesi and T. Lipper, *Adv. Funct. Mat.*, 2017, **27**, 1605690.
20 F. Haydous, M. Döbeli, W. Si, F. Waag, F. Li, E. Pomjakushina, A. Wokaun, B. Gökce, D. Pergolesi and T. Lipper, *ACS Appl. Energy Mater.*, 2019, **2**, 754–763.
21 A. Kudo, A. Tanaka, K. Domen, T. Onishi, *J. Catal.*, 1988, **111**, 296–301.
22 F. Wu, G. Liu and X. Xu, *J. Catal.*, 2017, **346**, 10–20.
28 D. L. Erbes and R. H. Burris, *Biochim. Biophys. Acta*, 1978, **525**, 45–54.
29 A.-M. Manke, K. Geisel, A. Fetzera and P. Kurz, *Phys. Chem. Chem. Phys.*, 2014, **16**, 12029–12042.
30 K. Maeda and K. Domen, *Chem. Mater.*, 2010, **22**, 612–623.
31 K. Maeda, T. Takata, M. Hara, N. Saito, Y. Inoue, H. Kobayashi and K. Domen, *J. Am. Chem. Soc.*, 2005, **127**, 8286–8287.
32 K. Maeda, K. Teramura, T. Takata, M. Hara, N. Saito, K. Toda, Y. Inoue, H. Kobayashi and K. Domen, *J. Phys. Chem. B*, 2005, **109**, 20504–20510.
33 S. Oros-Ruiza, R. Zanella, R. López, A. Hernández-Gordillo and R. Gómez, *J. Hazard Mater.*, 2013, **263P**, 2–10.
34 J. A. Navio and F. J. Marchena, *J. Photochem. Photobiol. A: Chem*., 1991, **55**, 319–322.
35 Y. Nosaka and M. A. Fox, *Langmuir*, 1987, **3**, 1147–1150.
36 Y. Nosaka and M. A. Fox, *J. Phys. Chem.*, 1988, **92**, 1893–1897.
37 T. Nakahira and M. Grätzel, *J. Phys. Chem.*, 1984, **88**, 4006–4010.
38 J. Sabaté, S. Cervera-March, R. Simarro and J. Giménez, *Int. J. Hydrogen Energy*, 1990, **15**, 115–124.
39 M. Wang, S. Shen, L. Li, Z. Tang and J. Yang, *J. Mater. Sci.*, 2017, **52**, 5155–5164.
23 S. Balaz, S. H. Porter, P. M. Woodward and L. J. Brillson, *Chem. Mater.*, 2013, **25**, 3337–3343.
24 W.-J. Chun, A. Ishikawa, H. Fujisawa, T. Takata, J. N. Kondo, M. Hara, M. Kawai, Y. Matsumoto and K. Domen, *J. Phys. Chem. B*, 2003, **107**, 1798–1803.
25 Y. Imanaka, T. Anazawa, T. Manabe, H. Amada, S. Ido, F. Kumasaka, N. Awaji, G. Sánchez-Santolino, R. Ishikawa and Y. Ikuhara, *Sci. Rep.*, 2016, **6**, 35593.
26 M. Ni, M. K. H. Leung, D. Y. C. Leung and K. Sumathy, *Renew. Sustain. Energy Rev.*, 2007, **11**, 401–425.
27 O. L. Stroyuk, O. Ye Rayevska, A. V. Kozytskiy and S. Ya Kuchmiy, *J. Photochem. Photobiol. A*, 2010, **210**, 209–214.
40 Y. Pellegrin and F. Odobel, *C.R. Chim.*, 2017, **20**, 283–295.
41 U. Pal, S. Ghosh and D. Chatterjee, *Transition Met. Chem.*, 2012, **37**, 93–96.
42 A. F. Alkaim, T. A. Kandiel, R. Dillert and D. W. Bahnemann, *Environ. Technol.*, 2016, **37**, 2687–2693.
43 K. Kalyanasundaram, J. Kiwi and M. Grätzel, *Helv. Chim. Acta*, 1978, **61**, 2720–2730.
44 K. Maeda, K. Teramura, D. L. Lu, T. Takata, N. Saito, Y. Inoue and K. Domen, *Nature*, 2006, **440**, 295.
45 A. Leelavathi, B. Mukherjee, C. Nethravathi, S. Kundu, M. Dhivya, N. Ravishankar and G. Madras, *RSC Adv.*, 2013, **3**, 20970–20977.
46 P. Maruthamuthu, S. Muthu, K. Gurunathan, M. Ashokkumar and M. V. C. Sastri, *Int. J. Hydrogen Energy*, 1992, **17**, 863–866.
47 H. Hagiwara, M. Nagatomo, C. Seto, S. Ida and T. Ishihara, *J. Photochem. Photobiol. A*, 2013, **272**, 41–48.
48 H. Hagiwara, R. Kakigi, S. Takechi, M. Watanabe, S. Hinokuma, S. Ida and T. Ishihara, *Surf. Coat. Tech.*, 2017, **324**, 601–606.
49 T. Watanabe and K. Honda, *J. Phys. Chem.* 86 (1982) 2617–2619.
50 P. W. King, M. C. Posewitz, M. L. Ghirardi and M. Seibert, *J. Bacteriol.*, 2006, **188**, 2163–2172.